

# Light-Field Microscopy with a Consumer Light-Field Camera

Lois Mignard-Debise  
INRIA, LP2N  
Bordeaux, France

Ivo Ihrke  
INRIA, LP2N  
Bordeaux, France

<http://manao.inria.fr/perso/~lmignard/>

## Abstract

*We explore the use of inexpensive consumer light-field camera technology for the purpose of light-field microscopy. Our experiments are based on the Lytro (first generation) camera. Unfortunately, the optical systems of the Lytro and those of microscopes are not compatible, leading to a loss of light-field information due to angular and spatial vignetting when directly recording microscopic pictures. We therefore consider an adaptation of the Lytro optical system.*

*We demonstrate that using the Lytro directly as an ocular replacement, leads to unacceptable spatial vignetting. However, we also found a setting that allows the use of the Lytro camera in a virtual imaging mode which prevents the information loss to a large extent. We analyze the new virtual imaging mode and use it in two different setups for implementing light-field microscopy using a Lytro camera. As a practical result, we show that the camera can be used for low magnification work, as e.g. common in quality control, surface characterization, etc. We achieve a maximum spatial resolution of about  $6.25\mu\text{m}$ , albeit at a limited SNR for the side views.*

## 1. Introduction

Light-field imaging is a new tool in the field of digital photography. The increasing interest is shown by the recent development of several hardware systems on the consumer market (Lytro, Raytrix, Picam), and applications in the research domain (stereo-vision, panoramic imaging, refocusing). The commercial systems are reliable, functional and inexpensive. However, they are designed for the imaging of macroscopic objects. In this article, we explore the use of commercial light-field cameras for microscopic imaging applications.

The light-field microscope has been introduced and improved by Levoy et al. [9, 10, 2]. While its conceptual details are well understood, its practical implementation relies on the fabrication of a custom micro-lens array, which

presents a hurdle for experimenting with the technology. In this article, we demonstrate the use of the Lytro camera, an inexpensive consumer-grade light-field sensor, for microscopic work. We achieve an inexpensive and accessible means of exploring light-field microscopy with good quality, albeit at a reduced optical magnification.

As we show, the major problem in combining the Lytro and additional magnification optics (in addition to f-number matching), is the loss of information due to spatial vignetting. Our main finding is the possibility of using the Lytro in what we term an *inverse regime*: in this setting the camera picks up a virtual object that is located far behind its imaging optics. To our knowledge, this is the first time that such a light-field imaging mode is described.

We investigate two different setups based on this inverse regime that do not suffer from spatial vignetting: 1) Our first option enables the use of the Lytro camera in conjunction with an unmodified microscope by designing an optical matching system. 2) The second option uses the Lytro behind a standard SLR lens in a macrography configuration to achieve macro light-field photography.

The paper is organized as follows. In Section 3, we study the compatibility of both optical systems involved in the imaging process: the light-field camera and the microscope. We discuss the implications of the combination of both systems in terms of both spatial and angular resolution. We then explore the Lytro main optical system and show how to adapt it to the microscopic imaging context, Sects. 5 and 6. Finally, we evaluate and compare the different solutions and present application scenarios, Sect. 7.

## 2. Related Work

**Light-field imaging** requires the acquisition of a large number of viewpoints of a single scene. Two types of approaches exist, either using multiple sensors or a single sensor in conjunction with temporal or spatial multiplexing schemes.

Taking a picture with a conventional camera is similar to a 2D slicing of the 4D light-field. Repeating this operation with a planar array of cameras offers sufficient data to esti-

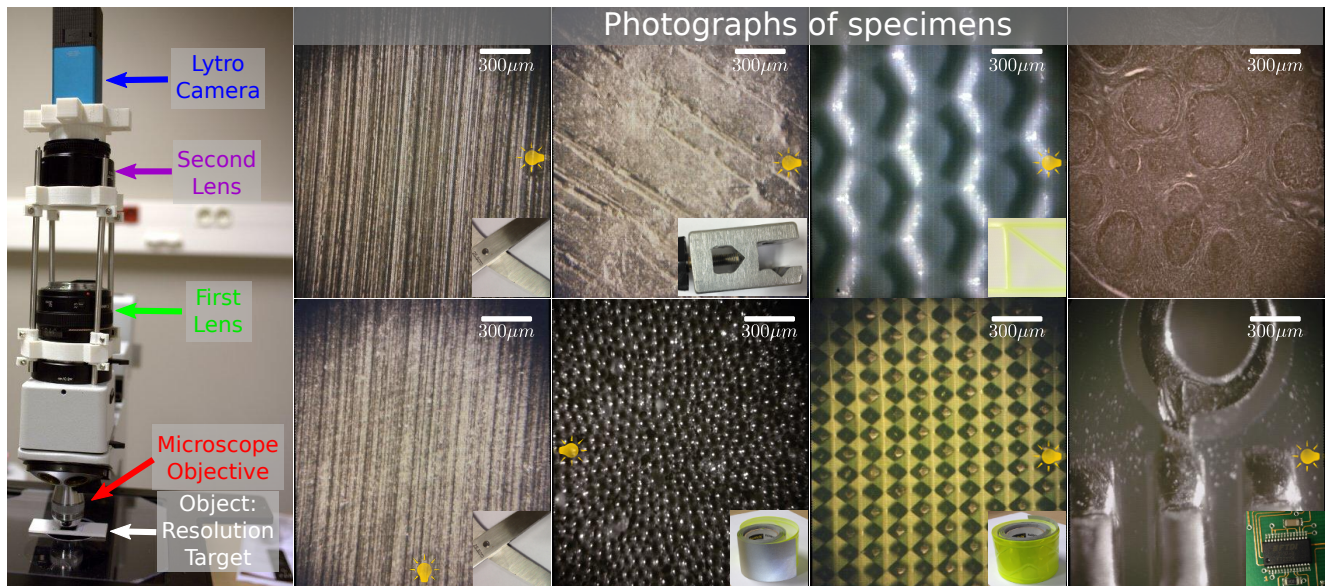


Figure 1. *Left*: Microscope setup with the Lytro camera on top of two additional SLR lenses. Images of several samples have been taken under different illumination conditions. Magnification is 3.0. *Top and bottom left*: brushed steel from scissors blade with lighting from the right and bottom. *Top middle left*: Scratched surface of a piece of metal. *Bottom middle left*: Plastic surface with highly retro-reflective properties. The material is made of micro bubbles of transparent plastic that are invisible to the naked eye. *Top middle right*: Fabric with a hexagonal structure. The lighting is coming from the side and casts shadows and strong highlights on the three-dimensional structure of the fabric. *Bottom middle right*: Highly retro-reflective material from security reflective tape. *Top right*: Tonsil tissue with bright field illumination. *Bottom right*: Pins of an electronic component on a circuit board.

mate the light-field function. Calibration, synchronization, as well as the available bandwidth of the camera hardware are the major determining features of this approach. More details can be found, e.g., in [25, 23]. The strongest limitation of this approach for microscopic applications is the large size of the corresponding setups.

An alternative method for light-field capture is to multiplex the different views onto a single sensor.

*Temporal multiplexing* is based on taking several pictures over time after moving the camera around static scenes. The movements can be a translation or rotation of the camera. Alternatively, mirrors [5, 19] can be moved to generate additional virtual viewpoints. Another alternative implementation are dynamic apertures [11].

*Spatial multiplexing* allows to record dynamic scenes. Parallax barriers and integral imaging [12] are historically the first approaches to spatially multiplex the acquisition of a light-field, trading spatial resolution for angular resolution. A modern elaboration of this approach where the sensor and a micro-lens array are combined to form an in-camera light-field imaging system is the Hand-Held Plenoptic Camera [17]. Alternatively, sensor masks [22, 21] or a light pipe [15] can be arranged such that in-camera light-fields can be recorded. Other methods use external arrays of mirrors instead of lenses [7], or external lens arrays [4].

**Microscopy** is a vast subject and many different illumination and observation schemes have been developed in the

past. A general overview is given in [16]; a comprehensive review of microscopy techniques, including light-field microscopy, for the neuro-sciences can be found in [24]. Light-field microscopy was introduced by Levoy et al. [9] and later augmented with light-field illumination [10]. Recently, addressing the large spatial resolution loss implicit in LFM, the group has shown that computational super-resolution can be achieved outside the focal plane of the microscope [2, 3]. Another super-resolution scheme is combining a Shack-Hartmann wavefront sensor and a standard 2D image to compute a high-resolution microscopic light-field [14]. LFM has been applied to polarization studies of mineral samples [18] and initial studies for extracting depth maps from the light-field data have been performed in microscopic contexts [8, 20]. Most of the work today uses the same optical configuration that was introduced in the original implementation [9]. With this article, we aim at providing an inexpensive means of experimenting with LFM.

## 3. Background & Problem Statement

### 3.1. Light-field Microscopy

The main function of an optical microscope is to magnify small objects so that they can be observed with the naked eye or a camera sensor. Light-field capabilities such as changing the viewpoint, focusing after taking the picture, and achieving 3D reconstruction of microscopic sam-

ples rely on the number of view points that can be measured from a scene. This number is directly linked to the object-side numerical aperture  $NA_o$  of the imaging system that is used as an image-forming system in front of the micro-lens array of the light-field sensor and the micro-lens f-number. The object-side numerical aperture is defined as

$$NA_o = n \sin(\alpha), \quad (1)$$

where  $n$  is the index of the material in object space (usually air, i.e.  $n = 1$ ). The numerical aperture quantifies the extent of the cone of rays originating at an object point and being permitted into the optical system (see Fig. 2). Microscope objectives usually have a high  $NA_o$ , because it is directly linked to better optical resolution and a shallower depth of field. A high  $NA_o$  is also important for light-field microscopy as the base-line of the light-field views is directly linked to it.

Details on how to design a light-field microscope can be found in [9]. The most important aspect is that the f-number of the micro-lens array matches the f-number of the microscope objective. The f-number  $F$  of any optical system is defined as the ratio of its focal length  $f$  over the diameter  $D$  of its entrance pupil (see Fig.2)

$$F = \frac{f}{D}. \quad (2)$$

For a microscope of magnification  $M_{microscope}$  and numerical aperture  $NA_o$ , a more appropriate equation taking the finite image distance into account can be derived [1] from Eq. 2:

$$F_{microscope} = \frac{M_{microscope}}{2NA_o}. \quad (3)$$

The majority of microscope objectives has an f-number between 15 and 40. In our experiments, we use a 10× objective with an f-number of  $F = 20$ .

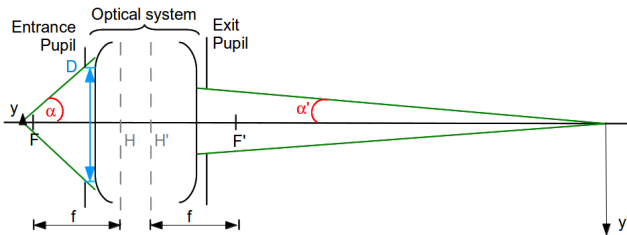


Figure 2. Properties of an optical system. An optical system is defined by its focal length  $f$ , its principal planes  $H$  and  $H'$ , and the diameter  $D$  of its entrance pupil. Two conjugate planes define a unique magnification  $M$ , the ratio of the image size  $y'$  over the object size  $y$ . All optical equations can be found in [1].

### 3.2. Lytro Features

The Lytro camera is made of an optical system that is forming an image in the plane of a micro-lens array that is, in turn, redirecting the light rays to a sensor. It has a  $3280 \times 3280$  pixel CMOS sensor with 12-bit A/D and

$1.4\mu m \times 1.4\mu m$  pixels [6]. Each micro-lens has a diameter of  $14\mu m$  which is equivalent to 10 pixels. The micro-lenses are packed on a hexagonal lattice (see Fig. 3 (left)). The effective spatial resolution is therefore  $328 \times 328$  pixels whereas the angular sampling rate is  $10 \times 10$  values. The Lytro’s main objective lens has a fixed f-number of  $F = 2$  and features an  $8 \times$  optical zoom. We explore its potential as an imaging parameter in Sect. 5. Another important feature of the objective lens is that it can focus from  $0mm$  to infinity.

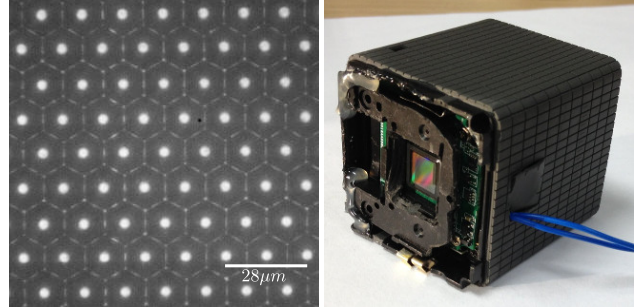


Figure 3. Left: Image of the micro-lens array taken with a microscope with top illumination. We can see the hexagonal structure of the micro-lens array. The bright dot in the middle of each hexagon is an image of the light source reflected by the surface of the micro-lens. Right: The Lytro camera without its optics.

### 3.3. F-number Mismatch

A prerequisite for non-vignetted imaging (see also Sect. 5) is that the f-number of the micro-lens array and that of the microscope objective match. This is the solution employed in conventional light-field microscopy [9, 18, 10]. A custom  $F = 20$  micro-lens array (MLA) is typically employed as it is compatible with a large number of existing microscope objectives. However, this  $F = 20$  MLA is not readily available and has to be custom manufactured.

Since the Lytro is designed for macroscopic imaging, its f-number ( $F = 2$ ) is not adapted to the microscopic situation. If we were to use the Lytro micro-lens array as is, the angular sampling in one direction would be divided by the ratio of the f-number of the two systems and only one pixel would be lit under each micro-lens (instead of approximately one hundred) (see Fig. 5 (bottom)). This would remove any interest for light-field purposes since only a single view would be recorded and 99% of the sensor would remain unused, see Sect. 5 for examples.

Therefore, in order to successfully use the Lytro camera for microscopic imaging, the f-numbers of the two optical systems need to be adapted. There is, however, a trade-off. The optical invariant, a fundamental law of optics (see e.g. [1]), states that for two conjugate planes, the product between the sine of the angle at which light rays reach a conjugate plane ( $\alpha$  and  $\alpha'$ ) and the size of the object in this

plane ( $y$  and  $y'$ ) is equal at both planes.

$$y n \sin(\alpha) = y' n' \sin(\alpha'), \quad (4)$$

$n$  and  $n'$  are the optical index of the media on both sides of the optical system. For air, the index is equal to 1.

We therefore opt for an optical demagnification scheme, decreasing  $y'$ , to increase the angular size of the cone of light rays  $\alpha'$  that is incident on the Lytro's light-field sensor. Theoretically, we need to divide the microscope objective's f-number by 10 to reach the same f-number as the Lytro camera. An immediate consequence from Eq. 3 is that the combination of all optical elements must therefore have a magnification divided by 10, i.e. we are aiming to convert the system to unit-magnification. Due to the small size of the Lytro's micro-lenses, the optical resolution of the system is still satisfactory, even at this low magnification (see Sect. 7).

The magnification of the combined system  $M_{final}$  can be written as the product of the magnifications of each individual system:

$$M_{final} = M_{microscope} M_{lens_1} \dots M_{lens_N} M_{Lytro}, \quad (5)$$

where  $M_{lens_i}, i=1..N$  indicates the magnification of  $N$  to-be-designed intermediate lens systems. The microscope objective has a fixed magnification of  $M_{microscope} = 10$ , whereas the lowest magnification setting of the Lytro has a value of  $M_{Lytro} = 0.5$ . The resulting  $M_{final} = 5$  without additional optical components ( $N = 0$ ) is too large to prevent angular information loss.

We explore two different options (see Fig. 4) to implement the adapted system. The first option (see Sect. 5) is to demagnify the image of the microscope with additional lenses ( $N = 2$ ). This solution lets us use the microscope and the Lytro camera unmodified. The second option is to remove the microscope, replacing it by an SLR lens in macro-imaging mode. Here, we compare a setup with and without the Lytro optics (see Sect. 6).

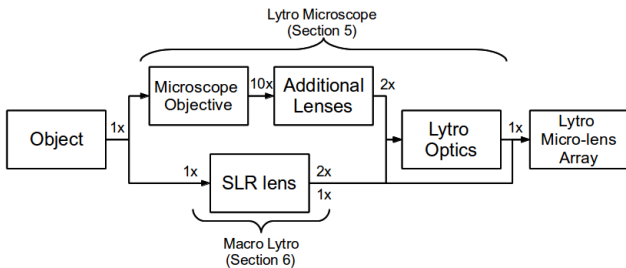


Figure 4. The diagram shows our two proposed solutions to achieve low magnification. The first option (first row) keeps the camera and the microscope intact. The second option (second row) replaces the microscope with an SLR lens.

## 4. Sensor Coverage

**Vignetting:** When using two or more optical systems in conjunction, some light rays are lost because the pupils of the different systems do not match each other. This effect is called vignetting. Generally, there are two types of vignetting: spatial and angular vignetting.

Spatial vignetting directly translates into a loss of field of view, which may reduce the image size at the sensor (see Fig. 5 (top)). Angular vignetting (see Fig. 5 (bottom)) occurs when the cone of rays permitted through one of the systems is smaller than for the other system, e.g. due to a stop positioned inside the system. Angular vignetting is not an issue in a standard camera : it only affects the exposure and is directly linked to the depth of field of the camera. In a light-field camera, however, it is crucial to minimize angular vignetting in order to prevent the loss of directional light-field information.

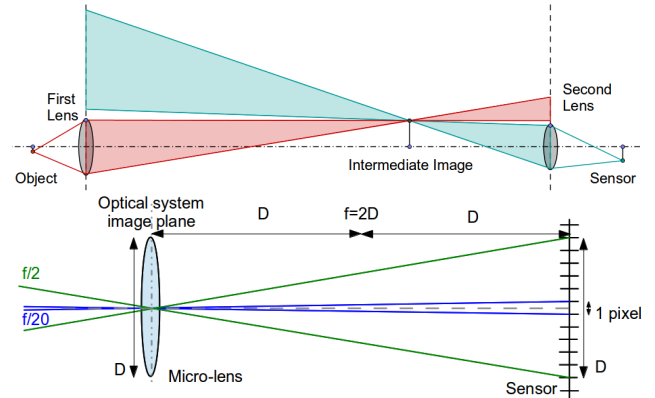


Figure 5. *Top:* Spatial vignetting occurs when light rays from the object (in red) do not pass through the second lens. For non-vignetted imaging, light rays (in blue) converging to a point at the sensor edge should include all the red light rays emerging from the object. *Bottom:* Representation of the sampling of a cone of light rays by a  $F = 2$  micro-lens. Green rays symbolize the angular cone that can be acquired by the micro-lens, while blue rays emerge from an  $F = 20$  optical system. As can be seen from the figure, angular vignetting prevents an effective sensor utilization.

We propose to measure the vignetting in terms of its adaptation to the recording light-field sensor. An ideal optical system that is adapted to a particular sensor would fully cover all its sensor elements. Since the raw pixel resolution is divided into spatial and angular parts, the sensor coverage  $c_{sensor}$  can be approximately expressed as

$$c_{sensor} [\%] = c_{spatial} [\%] \times c_{angular} [\%], \quad (6)$$

where  $c_{spatial}$  is the spatial coverage of the sensor in percent, and  $c_{angular}$  is the angular coverage of one micro-lens sub-image, also in percent. In our experimental validation, we measure the spatial coverage in the center view and the

angular coverage in the center lenslet. This choice is motivated by the simpler estimation of the relevant coverage areas as compared to using the side views/edges of the field. The measure can be considered to be an approximation of the upper bound of the system space-bandwidth product, i.e. the optical information capacity of the system [13].

#### 4.1. Unmodified Use of the Lytro's Main Optics

The main optics of the Lytro camera, i.e. the optics without the micro-lens array, is designed to avoid angular vignetting when imaging onto the micro-lens array, i.e. the micro-lens array and the main optics have been designed with the same f-number of  $F = 2$ . We have observed that the main optical system can be used in two different ways with a microscope. These two imaging regimes can be used differently in designing an optical matching system.

**Regular regime:** The Lytro camera can image a plane as close as the first surface of its optics for a zoom level of  $1\times$ . This minimal focus distance increases with the zoom level. In order to use the Lytro with the microscope, it has to be positioned such that the near focus of the camera is placed at the image plane of the microscope objective. Since the image size  $y'$  of the microscope objective is rather large (typically around  $50\text{mm} \times 50\text{mm}$ ) whereas the Lytro's entrance pupil is only  $\approx 20\text{mm}$  in diameter, spatial vignetting incurs a loss of sensor coverage of up to 94% as shown in Figure 7 (left). The angular vignetting is stronger with only 16% angular coverage.

**Inverse regime:** We discovered that, in a specific configuration where the camera is set to focus to the closest possible plane for a zoom level of  $1\times$ , the camera can enter into a virtual object regime. The camera is then able to image an object plane that is located *behind* its first lens, i.e. in the direction of the sensor (see Fig. 6). This configuration enables the positioning of the camera close to the microscope objective and therefore reduces the spatial vignetting since a larger number of rays can be captured by the lens surface (see Fig. 7 (right)). This mode of operation inverts the image.

For both imaging regimes described above, the magnification  $M_{Lytro} (\approx 0.5)$  is not low enough for achieving a good angular coverage. While the spatial vignetting problem can be successfully addressed with the inverse regime, the angular vignetting can only be dealt with by using a low magnification optical system. We therefore investigate the different options.

### 5. The Lytro Microscope

Our first option to achieve the matching of the f-numbers discussed in Section 3.3, consists in designing an optical de-

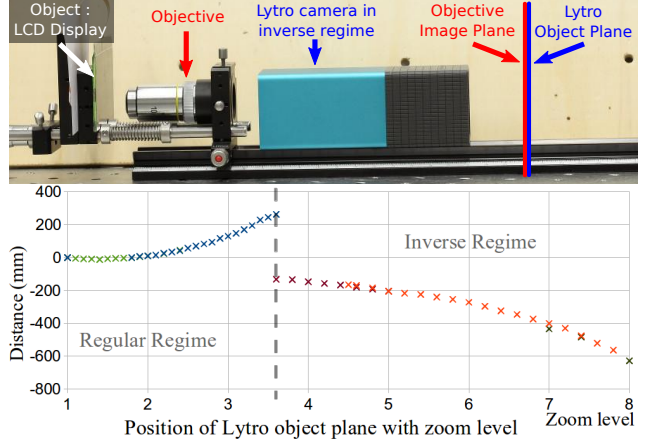


Figure 6. *Top:* Setup for the inverse regime configuration. *Bottom:* Distance of Lytro focus plane to its front lens with the variation of zoom. An abrupt change of position of the zoom lens group occurs for a zoom level of  $3.7\times$ , enabling to switch between the regular and inverse regime.

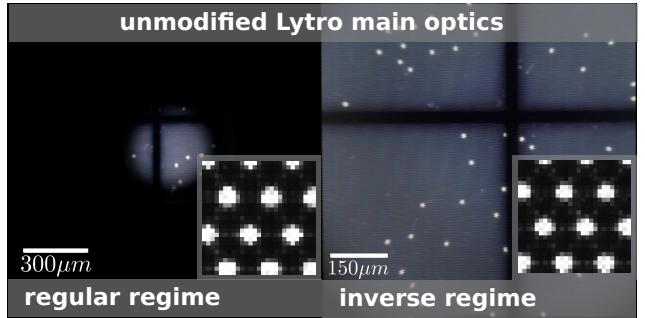


Figure 7. Direct imaging through a  $10\times$  microscope objective with an unmodified Lytro. The object is a blue LCD display. It consists of a square black grid that is separating the different pixels of  $0.5\text{mm} \times 0.5\text{mm}$  size. We hypothesize the white dots to be bubbles inside the liquid crystal. The large images show the equivalent camera image computed from the light-field, while the small images on the bottom right show a close-up on the micro-lens images of the raw sensor data for different zoom-levels. Spatial and angular vignetting are easily observed in the equivalent camera and micro-lens images, respectively. The zoom level setting is  $1\times$  (regular regime) on the left and  $5\times$  (inverse regime) on the right. The spatial vignetting is strong in the regular regime (6% of spatial coverage), while it is greatly improved in the inverse regime (100% of spatial coverage). Angular coverage is similar in both cases ( $c_{angular} \approx 25\%$ ).

magnification system (placed between the microscope objective and the Lytro) that increases the angular extent of the light (see Eq. 4). This solution keeps desirable properties like the large numerical aperture of the microscope and its fixed working distance, while at the same time, the Lytro camera can remain unmodified. The major task is to find a good trade-off between the vignetting and the magnification of the resulting light-field microscope.

Our best solution along this direction employs two lenses. This configuration serves two goals: 1) to decrease the magnification successively, simplifying the task of each individual lens, and 2) to move the image behind the Lytro camera so that it can be used in the inverse regime which offers a better spatial coverage  $c_{spatial}$ . The ray-diagram in Fig. 8 illustrates the two-lens setting: an intermediate image that is slightly demagnified is created in front of the microscope. Then, the second lens creates a further demagnified image behind the Lytro camera. The Lytro camera is operated in its inverse imaging regime in order to pick up this virtual image. We determine the positions and focal lengths of the additional lenses using the following equation derived from the thin lens formula:

$$x = f \frac{M - 1}{M} \quad (7)$$

The focal length  $f$  and the position of the lens  $x$  are chosen according to the desired magnification  $M$  (negative because the image is inverted). In our implementation, the first additional lens has a focal length of  $50\text{mm}$  and is put close to the microscope objective. The second additional lens has a focal length of  $85\text{mm}$  and is put close to the Lytro. The effect of using two lenses is that the individual focal lengths are larger and the aberrations are reduced.

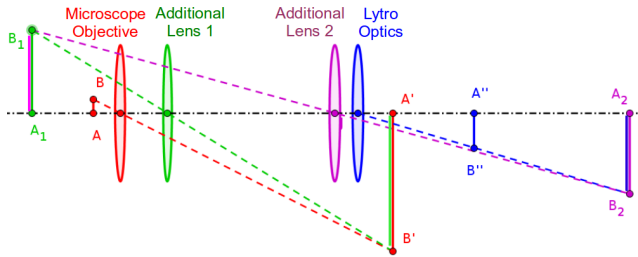


Figure 8. Ray-diagram of the system using two additional lenses. Each sub-system is indicated in a different color and has to be interpreted independently from the other sub-systems. Their operation can be understood in sequence: the objective images object  $AB$  to  $A'B'$ , the first additional lens images  $A'B'$  to  $A_1B_1$  so that the second lens images  $A_1B_1$  to  $A_2B_2$  behind the Lytro camera. Finally, the Lytro's main optics in the inverse regime images this virtual object  $A_2B_2$  to its sensor in the plane  $A''B''$ .

## 6. Macro Lytro

Our second option is to use a single SLR camera lens in front of the Lytro to achieve unit magnification. ( $M_{final} = M_{SLR}M_{Lytro} = 1$ ). As for the microscope, and because the focal length of the SLR lens is large ( $50\text{mm}$  and  $100\text{mm}$  in our experiments), we want to use the Lytro in the inverse regime to keep the spatial coverage as high as possible. In practice, the Lytro is set as close as possible to the SLR lens. A variation of this setup is to remove the Lytro optics, and only use the SLR lens so that  $M_{final} = M_{SLR} = 1$ .

These designs have only one or two optical components and relieve the hurdle of undoing the work of the microscope objective with many lenses. However, the SLR lens is not specifically designed for the magnification of close objects and its aperture is not meant to be maintained at a constant value for the micro-lens array. The relations used to establish Eq. 3 are not valid in this macro-configuration. Instead, the relevant quantity is the working f-number  $F_w$  [1] which is the f-number modified by the magnification  $M$ :

$$F_w = \frac{1}{2NA_i} = (1 - M)F \quad (8)$$

where  $NA_i$  is the image-side numerical aperture  $NA_i = n' \sin \alpha'$ . The minimal value of working f-number that can be achieved with a camera lens is close to  $F_w = 2$ . It is reached for a limit f-number of  $F = 1$  and a magnification of  $M = -1$ . This condition would be optimal for the Lytro micro-lens array. However, commercial lenses usually have a limit f-number between 1.4 and 3.5 increasing the working f-number to between 2.8 and 7.0.

Compared to the light-field microscope, on the one hand, this setup is more versatile. The magnification can be set to the desired value by simply moving the object and the micro-lens array. It does not require the difficult alignment of several optics. On the other hand, this setup does not benefit from the structure of the microscope that already includes lighting and moving the sample through micrometer stages in three dimensions. In addition, the working distance is not fixed which changes the magnification as well as the object-side numerical aperture when moving the sample. However, the strong point of this design is its accessibility. Building a light-field macrography setup is done quickly and without the need for a deep understanding of the operating principles of a microscope.

## 7. Results

Before showing results, we describe and compare the different implementations. The different sensor coverages as well as their spatio-angular coverage values can be found in Fig. 9. It is clearly visible that directly using the Lytro camera in its regular imaging regime is unsuitable for microscopic light-field imaging. The inverse imaging regime improves on the spatial coverage, but the angular coverage is limited. The best combination is achieved with a  $50\text{mm}$  SLR lens in front of the Lytro which yields the best overall sensor coverage  $c_{sensor}$ .

### 7.1. Resolution Test Chart

In order to compare the resolution of the two different techniques, we use a 1951 USAF resolution test chart. The results of the experiments are summarized in Fig. 10.

The first option (Sect. 5) "Lytro Microscope" was implemented using a  $50\text{mm}$  SLR lens and a  $85\text{mm}$

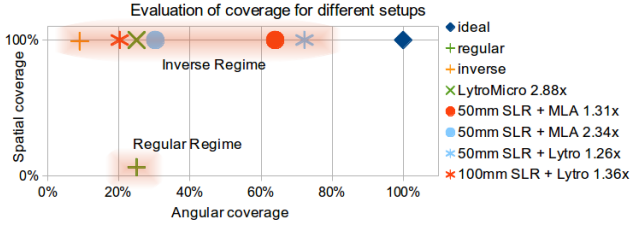


Figure 9. Combined results of the experiments from Sect. 5 and Sect. 6.

Setup	Magnification	Resolution (lp/mm)		Microlens footprint ( $\mu\text{m}$ )
		Measured	Theoretical	
Lytro Microscope	2.88	80	103	4.87
50mm SLR + MLA	1.31	32	47	10.7
50mm SLR + MLA	2.34	51	84	5.99
50mm SLR + Lytro	1.26	32	45	11.1
100mm SLR + Lytro	1.36	36	49	10.3

Figure 10. This table summarizes the results from the experiments of Sect. 5 and Sect. 6. Theoretical resolution is derived from the micro-lens pitch. The micro-lens footprint is the size of a micro-lens in object space.

SLR lens as additional lenses. Those lenses were put on top of a Leitz Ergolux microscope using an objective of magnification  $10\times$  with an object-side numerical aperture  $NA_o = 0.2$ . This microscope has a lens tube with a magnification of  $0.8\times$  so the f-number  $F = 20$ . The images have been taken with a magnification of 2.88, i.e. a micro-lens covers  $4.87\mu\text{m}$  in object space (see Fig. 11 (top)). The spatial coverage is above 99% but due to the large magnification the angular coverage is low (between 9% and 25%). The resolution is between 80 and 90 line pairs per  $\text{mm}$ .

The resolution indicated above is computed for the center view. It decreases with further distance from the center. A loss of image quality due to aberrations can be observed. They are introduced because the observed area is larger than usual for the microscope objective. Microscope objectives are typically designed so that only a reduced inner portion of the full field is very well corrected. In addition, our matching lenses introduce further aberrations. Since the angular vignetting is strong, the contrast of viewpoints far from the center is low. It should be noted that even viewpoints inside the vignetted area can be computed, albeit at a poor signal-to-noise ratio (see Fig. 11).

The second option (Sect. 6) was implemented in three ways: two times with the Lytro placed behind two different lenses, a 50mm and a 100mm Canon SLR lens (referred as SLR + Lytro), and with the Lytro micro-lens array without the Lytro main optics, see Fig. 3 (right), placed behind the 50mm lens (referred as SLR + MLA) (see Fig. 12). Magnifications from 1.26 to 2.34 were achieved. The spatial coverage is always 100% and angular coverage is good (up to 70%). In this case, chromatic aberrations are present which

degrades the image. The aberrations are reduced in the SLR + Lytro case as compared to SLR + MLA, since the magnification of the SLR lens is lower in this setting. It is most noticeable in the side views since, for these views, imaging is performed through the outer pupil regions of the SLR lens. We suspect that the chromatic aberration is introduced by the SLR lens because it is not intended for macro-imaging. Using a dedicated macro-lens instead would likely remove this effect.

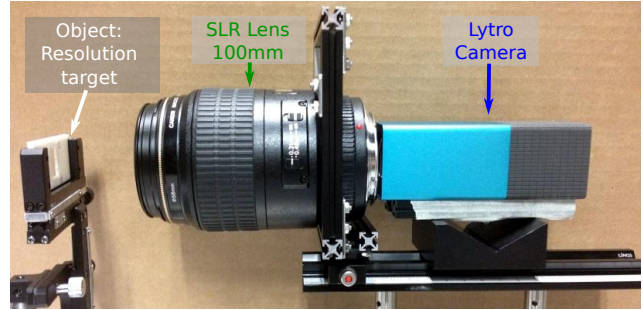


Figure 12. Setup from the SLR + Lytro experiment using a 100mm SLR lens (100mm SLR + Lytro).

## 7.2. Microscopic Sample

The most direct application of the light-field microscope is the study of microscopic samples. The low magnification and the large field of view allow us to see in detail an object area that is between  $1.5\text{mm} \times 1.5\text{mm}$  and  $3.5\text{mm} \times 3.5\text{mm}$  with a magnification of  $2.88\times$  and  $1.3\times$  respectively. Cell tissues or rough surfaces of different materials have a structure close to the millimeter so high magnification is not always necessary to analyze them.

We illustrate this technique in Fig. 1 (right). Several images of microscopic specimen were taken with the same settings as in the previous section. The magnification is  $2.88\times$  and we can clearly see the structure of different kind of surfaces that are invisible to the naked eye.

The light-field data allows for the reconstruction of the depth of the sample when the number of views is sufficient. We took a picture of a ground truth aluminium staircase with stairs of  $1.00\text{mm}$  width and  $0.50\text{mm}$  height with an accuracy of  $\pm 5\mu\text{m}$  with the 50mmSLR + Lytro setup. We obtained the depth map in Fig. 13 using a modified variational multi-scale optical flow algorithm for light-field depth estimation [15]. Although only a small slice of the staircase is in focus (the depth of field is  $1\text{mm}$ ), the depth can be computed outside of this area. Essentially, out-of-focus regions are naturally considered as a different scale by the algorithm, so, the estimation of the depth of the closest and furthest steps is correct. This behavior nicely interacts with the scene properties since the parallax is larger in out-of-focus regions. The optical system can be seen as supporting the part of the algorithm that is handling large dis-

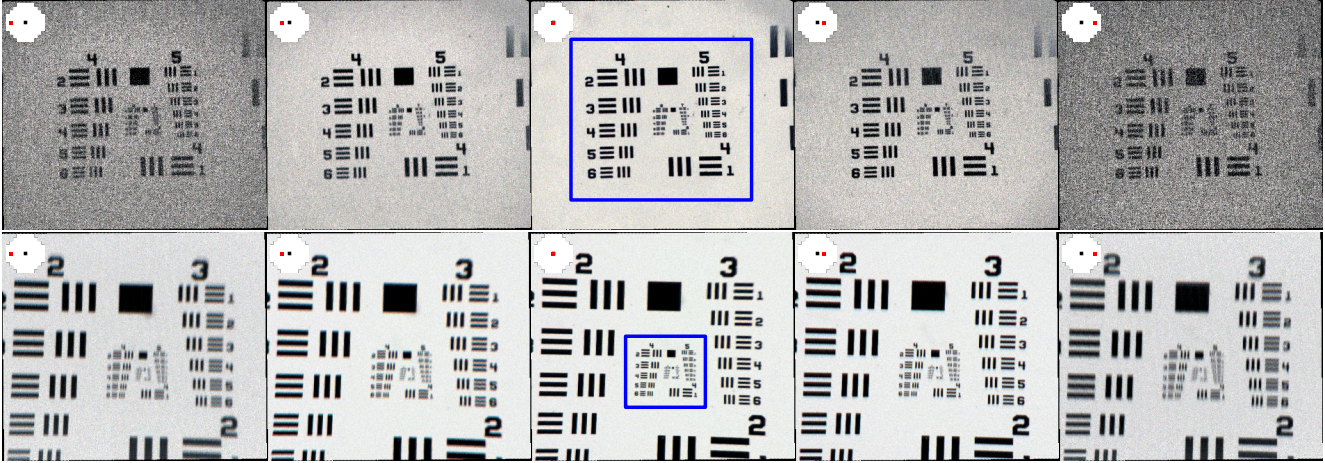


Figure 11. Set of different viewpoints of the resolution target with the center view in the middle (the red dot in the top left inset indicates the position of the view). *Top*: Images taken with the "Lytro Microscope" (Sect. 5). The magnification is 2.88. *Bottom*: Images taken with the "50mmSLR + Lytro" (Sect. 6). A red-green color shift due to strong chromatic aberrations can be observed in the side views. Note that the top row has a higher resolution: it shows the pattern that is visible in the center of the bottom row (level 4 and 5). The contrast of the images of the same row have been set to a similar level for comparison.

placements. Since the detailed properties of the Lytro main optics are unknown, it is necessary to adjust the scale of the computed depth. We use the aluminium staircase as reference. We find the affine transformation between the depth map and the staircase model by fitting planes to match the stairs. After the transformation, we measure an RMS error of  $75\mu\text{m}$  for vertical planes and  $17\mu\text{m}$  for horizontal planes. The difference is due to the different slopes of the horizontal and vertical steps with relation to the camera view direction. The magnification is equal to 1.32. We also applied this depth reconstruction to a daisy head (see Fig. 13). In practice, the depth inside a cube of about  $3.5 \times 3.5 \times 3.5\text{mm}^3$  can be estimated, which is rather large for a microscopic setting.

## 8. Discussion and Conclusion

We have developed and tested several adaptations of the Lytro consumer light-field camera to enable an entry-level experimentation with light-field microscopy. While the fixed f-number of the Lytro's micro-lens array prevents its direct use with a standard microscope (regular regime), it is possible to trade the overall system magnification for light-field features and to avoid spatial vignetting with the inverse imaging regime. Lytro microscopy is therefore an option for low-magnification work as is common in industrial settings, or for investigations into the meso- and large-scale micro-structure of materials. Even though an optical magnification between 1 and 3, as achieved in this work, appears to be low, the small size of the micro-lenses still yields a decent optical resolution of up to  $6.25\mu\text{m}$  in object space which already shows interesting optical structures that are imperceptible by the naked eye.

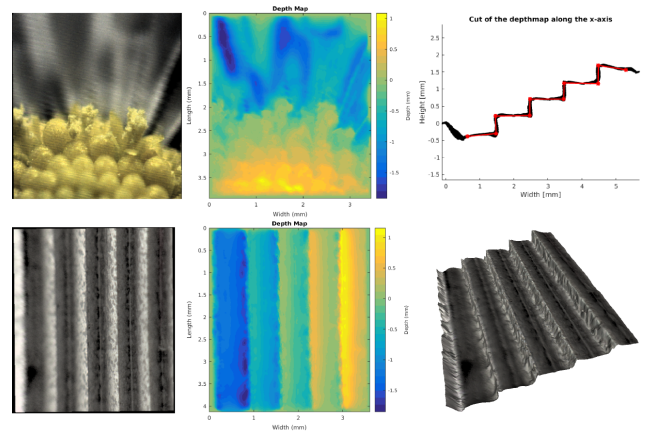


Figure 13. Sub-view (top left) and computed depth map (top middle) of a daisy flower. Sub-view (bottom left) and computed depth map (bottom middle) of the aluminium staircase. The bottom right picture is a 3D visualization of the depth map after the calibrating and the top right picture is a projection of a region in the middle of the calibrated depth map onto the  $xz$  plane showing the plane fits in red.

For the future, we would like to investigate image-based denoising schemes for the vignetted side-views, as well as algorithmic developments for structure recovery. In terms of applications, the imaging of micro- and meso-BRDFs and their relation to macroscopic BRDF models appears to be an interesting development.

## Acknowledgements

We would also like to thank Patrick Reuter for his helpful comments. This work was supported by the German Research Foundation (DFG) through Emmy-Noether fellowship IH 114/1-1 as well as the ANR



ISAR project of the French Agence Nationale de la Recherche.

## References

- [1] M. Born and E. Wolf. *Principles of optics*. Pergamon Press, 1980. 3, 6
- [2] M. Broxton, L. Grosenick, S. Yang, N. Cohen, A. Andalman, K. Deisseroth, and M. Levoy. Wave Optics Theory and 3-D Deconvolution for the Light Field Microscope. *Optics Express*, 21(21):25418–25439, 2013. 1, 2
- [3] N. Cohen, S. Yang, A. Andalman, M. Broxton, L. Grosenick, K. Deisseroth, M. Horowitz, and M. Levoy. Enhancing the performance of the light field microscope using wavefront coding. *Optics express*, 22(20):24817–24839, 2014. 2
- [4] T. Georgiev and C. Intwala. Light field camera design for integral view photography. Technical report, Adobe System, Inc, 2006. 2
- [5] I. Ihrke, T. Stich, H. Gottschlich, M. Magnor, and H.-P. Seidel. Fast incident light field acquisition and rendering. *Journal of WSCG (WSCG'08)*, 16(1-3):25–32, 2008. 2
- [6] J. Kučera. Lytro meltdown. <http://optics.miloush.net/lytro/Default.aspx>, 2014. 3
- [7] D. Lanman, D. Crispell, M. Wachs, and G. Taubin. Spherical catadioptric arrays: Construction, multi-view geometry, and calibration. In *3D Data Processing, Visualization, and Transmission, Third International Symposium on*, pages 81–88. IEEE, 2006. 2
- [8] J.-J. Lee, D. Shin, B.-G. Lee, and H. Yoo. 3D Optical Microscopy Method based on Synthetic Aperture Integral Imaging. *3D Research*, 3(4):1–6, 2012. 2
- [9] M. Levoy, R. Ng, A. Adams, M. Footer, and M. Horowitz. Light field microscopy. In *ACM Transactions on Graphics (TOG)*, volume 25, pages 924–934. ACM, 2006. 1, 2, 3
- [10] M. Levoy, Z. Zhang, and I. McDowall. Recording and Controlling the 4D Light Field in a Microscope using Microlens Arrays. *Journal of Microscopy*, 235:144–162, 2009. 1, 2, 3
- [11] C.-K. Liang, T.-H. Lin, B.-Y. Wong, C. Liu, and H. H. Chen. Programmable aperture photography: Multiplexed light field acquisition. *ACM Trans. on Graphics*, 27(3):1–10, 2008. 2
- [12] G. Lippman. Épreuves réversibles photographiques intégrales. *CR Acad. Sci*, 146:446–451, 1908. 2
- [13] A. W. Lohmann, R. G. Dorsch, D. Mendlovic, Z. Zalevsky, and C. Ferreira. Space-Bandwidth Product of Optical Signals and Systems. *Journal of the Optical Society of America A*, 13(3):470–473, 1996. 5
- [14] C.-H. Lu, S. Muenzel, and J. Fleischer. High-resolution Light-Field Microscopy. In *Computational Optical Sensing and Imaging*, pages CTh3B–2. Optical Society of America, 2013. 2
- [15] A. Manakov, J. Restrepo, O. Klehm, R. Hegedüs, H.-P. Seidel, E. Eisemann, and I. Ihrke. A Reconfigurable Camera Add-On for High Dynamic Range, Multispectral, Polarization, and Light-Field Imaging. *ACM Trans. on Graphics (SIGGRAPH'13)*, 32(4):article 47, 2013. 2, 7
- [16] D. B. Murphy and M. W. Davidson. *Fundamentals of Light Microscopy and Electronic Imaging*. John Wiley & Sons, 2012. 2
- [17] R. Ng, M. Levoy, M. Brédif, G. Duval, M. Horowitz, and P. Hanrahan. Light field photography with a hand-held plenoptic camera. *Computer Science Technical Report CSTR*, 2(11), 2005. 2
- [18] R. Oldenbourg. Polarized Light Field Microscopy: An Analytical Method using a Microlens Array to Simultaneously Capture both Conoscopic and Orthoscopic Views of Birefringent Objects. *Journal of Microscopy*, 231(3):419–432, 2008. 2, 3
- [19] Y. Taguchi, A. Agrawal, S. Ramalingam, and A. Veeraraghavan. Axial light field for curved mirrors: Reflect your perspective, widen your view. In *Computer Vision and Pattern Recognition (CVPR), 2010 IEEE Conference on*, pages 499–506. IEEE, 2010. 2
- [20] M. Thomas, I. Montilla, J. Marichal-Hernandez, J. Fernandez-Valdivia, J. Trujillo-Sevilla, and J. Rodriguez-Ramos. Depth Map Extraction from Light Field Microscopes. In *12th Workshop on Information Optics (WIO)*, pages 1–3. IEEE, 2013. 2
- [21] A. Veeraraghavan, R. Raskar, A. Agrawal, R. Chellappa, A. Mohan, and J. Tumblin. Non-Refractive Modulators for Encoding and Capturing Scene Appearance and Depth. In *IEEE Conference on Computer Vision and Pattern Recognition (CVPR)*, pages 1–8, 2008. 2
- [22] A. Veeraraghavan, R. Raskar, A. Agrawal, A. Mohan, and J. Tumblin. Dappled Photography: Mask Enhanced Cameras For Heterodyned Light Fields and Coded Aperture Refocussing. *ACM Trans. on Graphics (TOG)*, 26:69, 2007. 2
- [23] B. Wilburn, N. Joshi, V. Vaish, E.-V. Talvala, E. Antunez, A. Barth, A. Adams, M. Horowitz, and M. Levoy. High performance imaging using large camera arrays. In *ACM Trans. on Graphics (TOG)*, volume 24, pages 765–776. ACM, 2005. 2
- [24] B. A. Wilt, L. D. Burns, E. T. W. Ho, K. K. Ghosh, E. A. Mukamel, and M. J. Schnitzer. Advances in Light Microscopy for Neuroscience. *Annual Review of Neuroscience*, 32:435, 2009. 2
- [25] J. C. Yang, M. Everett, C. Buehler, and L. McMillan. A real-time distributed light field camera. In *Proceedings of the 13th Eurographics workshop on Rendering*, pages 77–86. Eurographics Association, 2002. 2